J. Appl. Comput. Mech., 12(1) (2026) 60-73
DOI: 10.22055/jacm.2025.47278.4687

ISSN: 2383-4536
jacm.scu.ac.ir

Shahid Chamran University of Ahvaz

Journal of Applied and Computational Mechanics

Research Paper

Application of Acoustic Emission for Diagnostic Pile Penetration by Consideration of Soil Particle Breakage

Mohammad Rostami[1], Abdolghafour Khademalrasoul[1], Ali Valipour[2]

[1] Faculty of Civil Engineering and Architecture, Shahid Chamran University of Ahvaz, Ahvaz, Iran,
Email: m-rostami@stu.scu.ir (M.R.); ag.khadem@scu.ac.ir (A.Kh.)

[2] Department of Mechanical Engineering, Faculty of Engineering, Shahid Chamran University of Ahvaz, Ahvaz, Iran, Email: a.valipour@scu.ac.ir

Received June 26 2024; Revised April 01 2025; Accepted for publication April 02 2025.
Corresponding author: A. Khademalrasoul (ag.khadem@scu.ac.ir)

Abstract. The possibility of passive monitoring on penetrating structural piles through acoustic signals is presented. The purpose of this study is first to provide deeper understanding on different situations against pile penetration into the soils through insights of acoustic emission technique. During pile installation, the soil under and surrounding the piles is overstressed, causing particle slippage and breakage. Due to the particle breakage the elastic acoustic wave propagates throughout the domain. Following the validation of the numerical simulation through a comparison of the available experimental evidences, a parametric study was performed to evaluate the acoustic signals during pile penetration accompanied by particle breakage and slippage. In this contribution, an extensive numerical simulation is conducted considering the influential parameters onto the signals propagated during pile driving. The studied parameters included pile materials, soil modulus of elasticity, and different obstacles or voids under pile tip. Moreover, the role of the dynamic soil-pile-interaction was assessed using acoustic signal interpretation. The results indicate that, all influential parameters have significant effects on the observed signals. The findings of this study provide valuable information regarding the effects of different underground circumstances for designers.

Keywords: Particle breakage, Acoustic signal, Pile penetration, Soil-structure interaction.

1. Introduction

The study of mechanical properties of soil subjected to high stress is of great concern in soil mechanics. When stresses resulting from external pressures exceed the resistance of particles or the resistance at the interparticle contacts, soil particles become susceptible to breakage. This will affect the soil's resistance and mechanical properties. Particle breakage and its impact on soil behavior have been comprehensively investigated in previous studies [1, 2]. In the field of geotechnical engineering, particle breakage occurs in various scenarios including dam foundations and large embankments [3], the soil surrounding pile tips[4], and natural disasters like rockslides [5]. The effect of soil particle breakage beneath the tip of a pile can be easily discerned through close observations (in the field and with the naked eye). Generally, based on field measurements and laboratory tests, a lower bearing capacity is expected for soil that has undergone particle breakage. Although various approaches have been suggested for assessing the bearing capacity of soil subjected to particle breakage, the theoretical backgrounds and assumptions of these approaches vary widely, such as the spherical cavity method proposed by [6], the relative breakage surface method suggested by[7], the discrete element method proposed by [8], the breakage mechanics theory extended by [9] , and the finite element simulation method proposed by [10]. The most common laboratory method for assessing particle breakage is the measurement of grain size distribution after drilling or excavation. However, measuring grain size distribution is limited to post-test characteristics, with the related properties during the particle breakage process remaining unknown.

This research is distinct from previous studies in that it focuses on the energy radiated from sands subjected to loading induced by the penetration of a pile. In the case of pile installation operations, the soil around the pile shaft and beneath the pile tip experiences stress, and energy is released as elastic waves due to the sliding of particles against each other or their breakage. These elastic waves are known as acoustic emissions.

Acoustic Emission (AE), as a prominent non-destructive testing (NDT) method, has been utilized for many years to detect the initiation and propagation of damage in various materials and structures. In fact, AE is valuable for characterizing material behavior [11], identifying damage [12], predicting destruction and estimating the remaining useful life of structures [13], Moreover AE was used to monitor ancient structures against seismic hazards [14], and diagnose structural damage in historical buildings [15]. The advantage of the AE method over other non-destructive tests lies in its high sensitivity and non-invasiveness. Non-destructive tests are classified into two categories: active and passive, depending on the input energy of the system. While active techniques, such as radiography and ultrasonic, display recorded signals based on the energy applied to the inspected sample, passive techniques encompass tests that do not require input energy to elicit a response but rather rely on the structure's response to external loads, such as fracture [16], plastic deformation[17], and corrosion [18].

Published online: April 05 2025

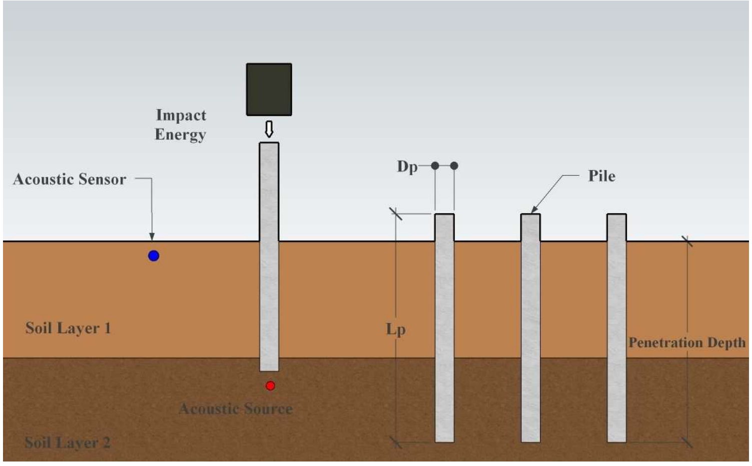

Fig. 1. Penetrating pile and waves emanating from pile penetration in the soil.

Despite the advantages mentioned for AE and significant advancements in the fields of hardware (sensor technology) and software (signal processing), its transition from a laboratory method to a practical approach for Structural Health Monitoring (SHM) still faces challenges. Among the primary obstacles that have hindered the widespread adoption of AE, insufficient quantitative assessment and validation of recorded laboratory signals can be highlighted. The main challenge in the development and quantitative assessment of AE can be attributed to the relatively complex waveforms resulting from the effects of energy radiated from the initiation point of damage in the acoustic emission source. Another major challenge associated with AE is the difficulty in interpreting the nature of AE information utilizing source inversion methods, referred to as the inverse problem. Therefore, the separation of genuine signals from unwanted noise signals is currently achieved through advanced signal processing[19], statistical pattern recognition approaches[20], and data fusion methods [21].

Cutting-edge studies regarding to particle breakage in the field of AE have been conducted by [22]. In their study[23], they have investigated the location of particle breakage in sandy soils using the acoustic emission technique. The localization of the AE source is achieved through mathematical analyses and operations on the obtained signals. During the propagation process, acoustic signals are attenuated by factors such as material type [24] and structural features [25]. Additionally, environmental factors introduce noise, posing challenges in the accurate localization of the acoustic source New methods have recently been developed in the field of acoustic source localization, some of which including the computational intelligence to detect the acoustic source [26] and using artificial intelligence to detect the onset time of signal propagation [27].

The current study aims at exploring the localization of particle breakage in soil using acoustic waves and investigating the influence of the sheared zone on acoustic signals. Furthermore, the effects of pile type, soil type, and the presence of obstacles in the path of pile on acoustic signals are investigated. The advantage of this approach lies in its applicability during pile-driving operations, where the operator can gain awareness of the soil and material conditions beneath the pile. This enables more optimized pile-driving operations by understanding the underlying soil type. Another advantage of this method is that, with a better understanding of the subsurface soil properties, the bearing capacity that the pile can effectively withstand can be calculated and compared using computational methods. Moreover, gaining insights into the soil-pile interaction during penetration is another valuable aspect of the proposed method. One of the most significant advantages of modeling compared to practical testing is the absence of noise in the received signals, eliminating the need for signal filtering. Additionally, it offers benefits such as reduced cost and time, increased accuracy, and access to a wide range of materials and testing conditions.

2. Acoustic Signal Evaluation Method and Source Localization

In the context of acoustic emission source localization, methods such as the calculation of the Time of Arrival (ToA) and the calculation of the Time Difference of Arrival (TDoA) can be employed. These approaches rely on the calculation of the distance between the sensor (receiver) and the source (transmitter). Whereas a minimum of three sensors is required for localization in a two-dimensional space, at least four sensors are necessary in a three-dimensional space. Increasing the number of sensors enhances the accuracy of localization. The Time of Arrival method utilizes the relationship between the distance and the signal transmission time, assuming the propagation speed is known. Assuming the transmitter and receiver know the transmission start time, the distance between two nodes can be calculated as $d = v \times t$ where d is the distance, v is the signal propagation speed, and t is the time it takes for the signal to reach the receiver from the moment of transmission. Since precise synchronization between the transmitter and receiver is necessary, any lack of synchronization will result in measurement errors. Another drawback of this method is that the propagation speed varies depending on the medium. Therefore, environmental conditions will impact the measurements. In the Time Difference of Arrival method, by placing one of the receivers as a reference, the time difference for the signal to reach the other receivers relative to the reference receiver is calculated. By processing these delays, the location of the target can be estimated. The first requirement for the accurate calculation of these delays is the synchronization of the receivers. To calculate the Time of Arrival (ToA) [28], the Akaike Information Criterion (AIC) [29] ,Standard Threshold-Crossing Technique [30] and using artificial intelligence [31] can be utilized. The Time Difference of Arrival (TDoA) [32] can be obtained from the differences between the calculated ToA values of each sensor. Other methods, including cross-correlation [33], generalized cross-correlation [34], wavelet covariance model [35] as well as other similar methods are also employed to calculate TDoA.

2.1. Cross-correlation

Calculating the difference in time-of-arrivals forms the basis, and is the key, of the TDoA localization technology, as its accuracy directly impacts the localization process. In this study, the cross-correlation approach has been employed to calculate the time delays. The cross-correlation function is described as Eq. (1):

$$R_{xy}(\tau) = \lim_{T \to \infty} \frac{1}{T} \int_0^T x(t)\, y(t+\tau)\, dt \tag{1}$$

Table 1. Fracture criterion of concrete

σ_{max} (MPa)	G_{IC} (N / m)	G_{IIC} (N / m)	G_{IIIC} (N / m)
10.45	19.58	19.58	19.58

where R_{xy} represents the correlation coefficient between two signals, and both x(t) and y(t) have the same duration. τ denotes the time delay, and T is the signal duration. The higher the correlation coefficient, the more similar the two signals are. As illustrated in Fig. 2, the time corresponding to the maximum value of the function represents the time difference between the two signals.

Based on the calculated TDoA, various algorithms can be utilized such as Spherical Interpolation (SI) [36], Spherical Intersection (SX) [37], Chan's Algorithm[38], Taylor Series [39], Weighted Least Squares [40], etc. In this study, we employed the Spherical Interpolation method. Before proceeding with the modeling, we will first validate the method. The validation process includes verifying the accuracy of simulating acoustic waves in the Abaqus software and validating the localization algorithm.

3. Numerical Validating

3.1. Validation of acoustic wave simulation method

To validate the acoustic wave simulation method, the laboratory model developed by [41] was first simulated using the Abaqus software. Subsequently, the simulation results were compared with the experimental outcomes. This experiment was conducted on several series of concrete beam specimens subjected to four-point bending tests. These specimens had dimensions of 1150 mm in length, 100 mm in width, and 150 mm in height (as shown in Fig. 3). Additionally, the 28-day compressive strength of the cylindrical specimen was 35 MPa. The specimens were reinforced with a #6 rebar (diameter of 19.05 mm) placed at a depth of 30 mm from the concrete surface. The concrete specimen was subjected to a four-point bending test, and as a result of loading, elastic waves were generated due to the formation of cracks in the specimen.

3.1.1. Simulation Steps

In the initial step, the geometry of the model was created in the Abaqus software (www.3ds.com/products/simulia). The concrete properties and its damage characteristics were derived from the research conducted by [42]. The concrete's Young's modulus was 31 GPa, and its density was 2400 kg/m^3. To simulate cracks, the Extended Finite Element Method (XFEM) [43] was utilized, for damage initiation the maximum principal stress failure is selected and for damage propagation an energy based damage evolution law based on power law fracture criterion is considered [42]. The related data is as followed:

To simulating the separation between concrete and rebar, the Cohesive Zone Model (CZM) [44] was employed. The properties of the CZM model were adopted from the research by[45]. Following parameters were used to explain the traction-separation behavior: $k_{nn} = 1500\,\text{Mpa/mm}$, $k_{ss} = 3600\,\text{Mpa/mm}$, $k_{tt} = 360\,\text{Mpa/mm}$. Maximum stress considered to damage initiation are: $t_n^0 = 110\,\text{MPa}$, $t_s^0 = 9\,\text{MPa}$, $t_t^0 = 9\,\text{MPa}$.

For this analysis, two dynamic explicit time steps have been employed. In the first step, the concrete beam is considered until the first crack happens. Then, the second step begins, where associated with the growth of the crack and the propagation of acoustic waves. The time duration for the second step is set to 400 microseconds with the increment size of 1 microsecond. The sampling frequency of acoustic wave signals should be at least twice the frequency of the acoustic signals in the material. According to the study by [41], the maximum frequency of acoustic waves in concrete is 400 kHz. For this purpose, in this modeling, the sampling frequency is set to 1 MHz. The reason for using these two-time steps is that, due to the absence of any wave propagation before the initiation of the crack, the analysis time is divided into two parts: before the crack initiation and after it. The most significant computational advantage of this assumption is related to the time increments during acoustic signals propagation. Hereupon, the time intervals are high and variable before the crack initiation and low and constant after the crack initiation. This modeling technique significantly reduces the computational analysis efforts. For discretizing acoustic waves, the smallest dimensions of finite element components should be between $\lambda / 12$ and $\lambda / 6$, where λ represents the wavelength. In this simulation, the smallest mesh size has been set to $\lambda / 8$. λ represents the wavelength and is calculated using the Eq. (2):

$$\lambda = \frac{v}{f} \tag{2}$$

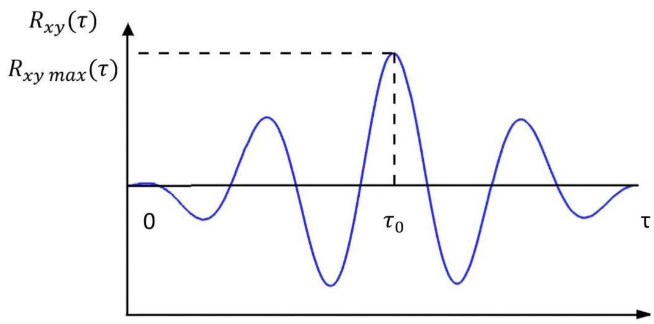

Fig. 2. Cross-correlation function plot.

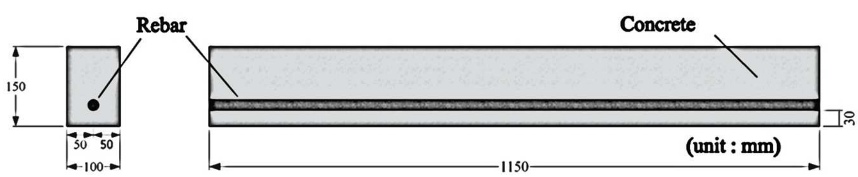

Fig. 3. Dimensions of the laboratory concrete beam specimen and rebar placement.

Table 2. Steel material properties.

Material type	Speed of sound (m/s)	Density (kg/m)	Poisson's ratio	Young's modulus (GPa)
Steel	6320	7870	0.29	200

where f represents the frequency of the acoustic signal, which is equal to 400 kHz, and υ is the acoustic wave velocity, which is defined by the Eq. (3) and Eq. (4):

$$\upsilon = \sqrt{E/\rho} = \sqrt{31.37\times10^{9}/2400} = 3615\, m/s \tag{3}$$

$$\lambda = \upsilon/f = 3615/400\times10^{3} = 0.00904\, m \tag{4}$$

Finally, the mesh size is determined by the Eq. (5):

$$\lambda/8 = 0.00904/8 = 0.00113\, m \tag{5}$$

3.1.2. Results of modeling verification

In order to validate the numerical simulation a reinforced concrete beam subjected to four point bending as shown in Fig. 4(a) considered. Figure 4(b) shows the Mises stress distribution in the modeled beam subjected to 4-point loading configuration. Figure 5 illustrates the received signal and its Fast Fourier Transform (FFT) representation in the experimental study, with a dominant frequency of 190 kHz. Figure 6 shows the received signal and dominant frequency in this numerical simulation. As Fig. 6 demonstrates, the dominant frequency of the received signal from the numerical modeling is 182 kHz, which, with slight discrepancies, aligns with the frequency of the received signal from the experimental model. Therefore, it can be concluded that the adopted method for simulating acoustic waves traveling through the reinforced concrete beam is accurate enough.

3.2. Validation of localization algorithm

In this section, an attempt has been made to validate the proposed localization method. Initially, an acoustic pulse is introduced into a specific point on the object. Then, the actual characteristics of the location of the pulse are compared with the calculated characteristics. The simulation of the steel plate is performed using the Abaqus software, and the validation of the localization method is carried out using the MATLAB software (www.mathwork.com). First, a steel plate with dimensions of 10 cm × 10 cm is created, for which the specifications are provided in Table 2.

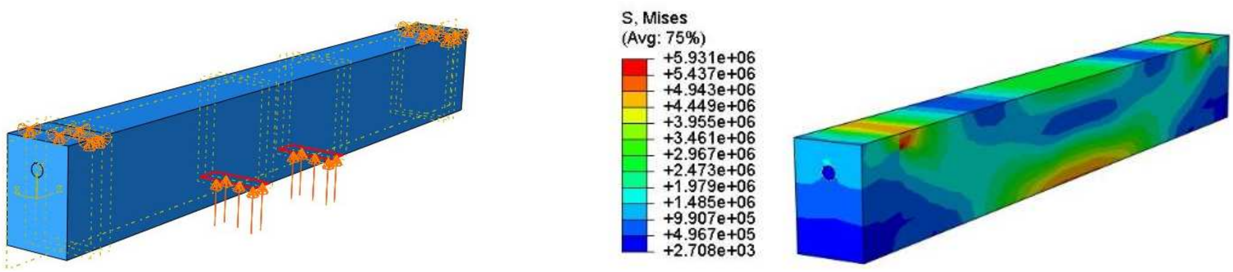

(a) (b)

Fig. 4. (a) four point bending setup, (b) Von Mises Stress distribution.

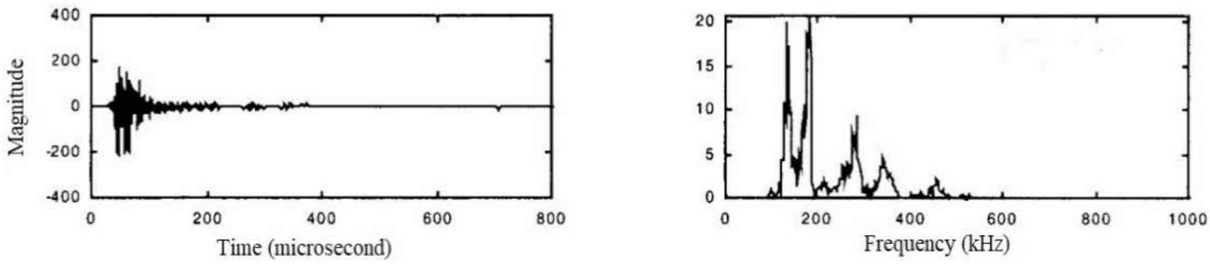

Fig. 5. Received signal and frequency domain representation from the experimental sample [41].

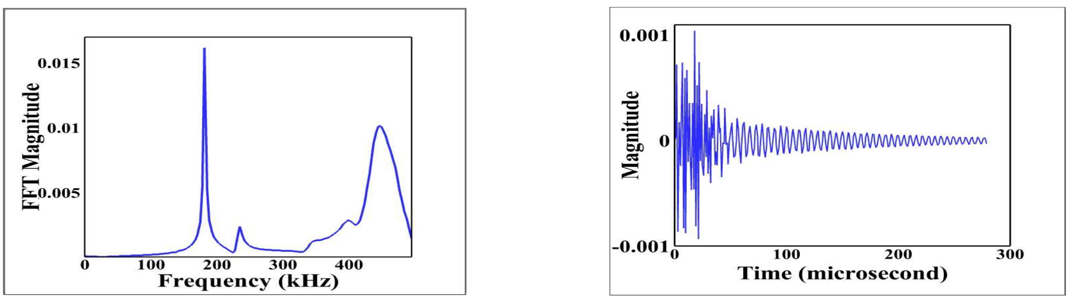

Fig. 6. Received signal and its FFT representation from the current study.

Next, an applied excitation to create a sound pulse is defined in the numerical simulation according to the Eq. (6) in terms of time:

$$A = \begin{cases} \left[1-\cos\left(\frac{2\pi f}{N}t\right)\right]\left(\cos(2\pi f t)\right) & 0 \le t \le \frac{N}{f} \\ 0 & t \ge \frac{3}{f} \end{cases} \tag{6}$$

In Eq. (6), f represents the excitation frequency, which is set to 1 MHz, and N denotes the number of cycles applied, assumed to be 3 in this problem, and A is be applied excitation amplitude. Figure 7 illustrates the applied excitation to generate the acoustic pulse.

The solution method employed in this study is explicit dynamic. The reason for using an explicit dynamic solver is that it avoids ineffective calculations and, consequently, the wasting of time, resulting in reduced computational volume and cost. Two crucial variables in analyzing acoustic problems are the time and the type/size of finite elements. The type of element chosen for this analysis is the four-node bilinear quadrilateral element with reduced integration and hourglass (CPE4R). As previously mentioned, in acoustic wave meshing, the smallest dimensions of finite element components must fall within $\lambda / 12$ to $\lambda / 6$. In this simulation, the smallest mesh size is set to $\lambda / 8$. Calculated using the Eq. (7):

$$\lambda/8 = 7.3625 \times 10^{4} \tag{7}$$

In the analysis of acoustic problems and wave propagation, the choice of time plays a critical role. Therefore, the total time for the analysis must be optimized to the best possible scenario. An excessively long analysis time prolongs the modeling process, while a too short time may not yield meaningful results. The total analysis time is calculated as follows, encompassing the time for the wave to reach the end of the plate, the duration of the acoustic pulse, and an additional time for error reduction. In this contribution, the total analysis time consists of three different components including as:

1. Time for the wave to reach the end of the plate is equal to Eq. (8):

$$t_1 = x/v = 0.01/6320 = 16\mu s \tag{8}$$

2. Time for the creation of an acoustic pulse is assumed as equal to Eq. (9):

$$t_2 = N/f = 3/10^6 = 3\mu s \tag{9}$$

3. Considering additional time for error reduction:

In this analysis, a duration of 6 microseconds has been considered for error reduction:

$$t_3 = 6\mu s$$

Therefore, the total analysis time is determined as equal to Eq. (10):

$$t_{total} = t_1 + t_2 + t_3 = 25\mu s \tag{10}$$

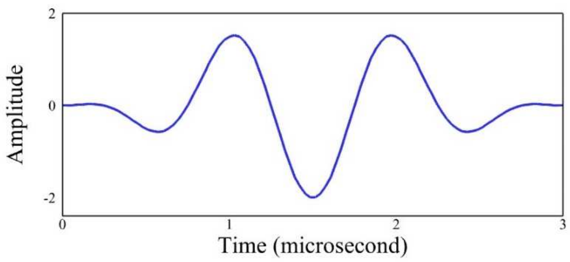

Fig. 7. Representation of the applied pulse excitation.

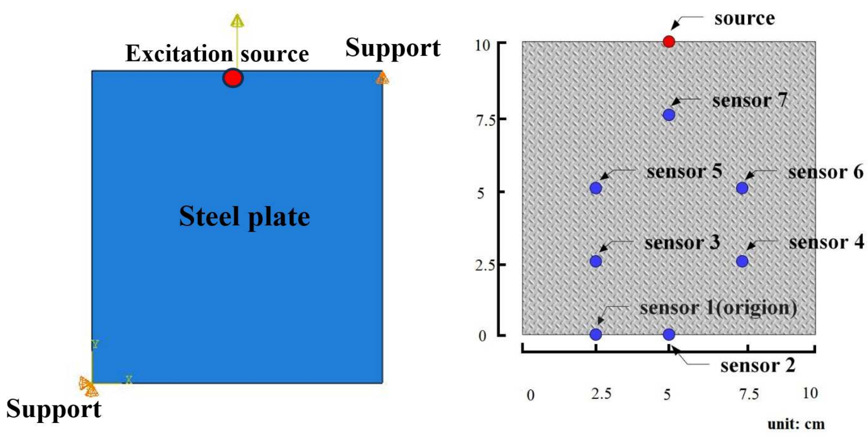

(a) (b)

Fig. 8. (a) Representation of the entry point of the pulse and boundary conditions, (b) Coordinates of the sensors and the acoustic source.

Table 3. Coordinates of sensors, acoustic source, and computational reference.

	X-Coordinate	Y-Coordinate
Sensor 1 (origin)	0.25	0
Sensor 2	0.75	0.03
Sensor 3	0.25	0.03
Sensor 4	0.75	0.03
Sensor 5	0.25	0.06
Sensor 6	0.75	0.06
Sensor 7	0.5	0.08
The precise location of acoustic source	0.5	0.1
The location of computational reference	0.494	0.1102

The applied pulse, as shown in Fig. 8, has been introduced into the plate as the source. The boundary conditions are set such that the plate is constrained horizontally and vertically at the bottom right corner and vertically at the top right corner (Fig. 8(a)). The coordinates of the acoustic source (location of the applied pulse) and the receiving sensors are illustrated in Fig. 8(b).

After applying the pulse at the specified point as shown in Fig. 8(a), the wave propagates in the plate, as depicted in Fig. 9. Signals received by the available sensors are then collected. For instance, the received signals from Sensor 2 and Sensor 4 are illustrated in Fig. 10.

For the localization process, Sensor 1 is initially chosen as the reference sensor. The time differences between the start of other signals concerning it are then calculated using cross-correlation method. Subsequently, the localization is performed using the Spherical Interpolation (SI) method. The coordinates of the sensors and the acoustic source, as well as those of the computational reference point, are listed in Table 3.

The calculations indicate that the coordinates of the acoustic source do not significantly differ from the coordinates of the computational reference point. With a very low error percentage, the computational location is highly accurate. Therefore, it can be concluded that the localization algorithm utilized in this study provides a remarkable level of accuracy and precision in estimating the position of the disturbed reference and wave propagation.

4. Diagnostic Pile Penetration using Acoustic Emission

4.1. Locating the interparticle breakage

In this contribution, due to the unknown nature of the acoustic wave emission in soils, an extensive numerical simulation is performed to obtain the acoustic waves in soil based on the experimental findings documented in existing research studies conducted by [23]. For this purpose, a box containing the silica sand with dimensions of 1600 mm × 1600 mm × 1200 mm including a penetrating aluminum pile with 40 mm diameter and 1000 mm long, with 550 mm of its length buried inside a silica sand, as depicted in Fig. 11 and Fig. 12, is modeled to move into the soil.

In the laboratory experiments related to the investigation of particle breakage, silica sand and carbonate sand have mainly been utilized. Silica sand is chosen due to the significant acoustic signals generated as a result of particle fragmentation and slippage, making it more suitable for acoustic source localization compared to carbonate sand [46].

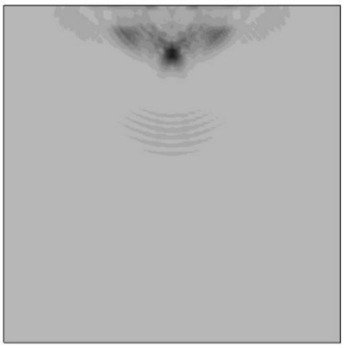

Fig. 9. Wave propagation inside the body.

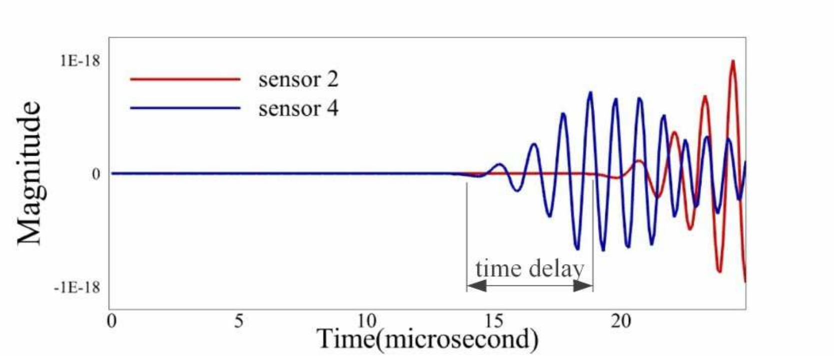

Fig. 10. Received signals from sensors 2 and 4.

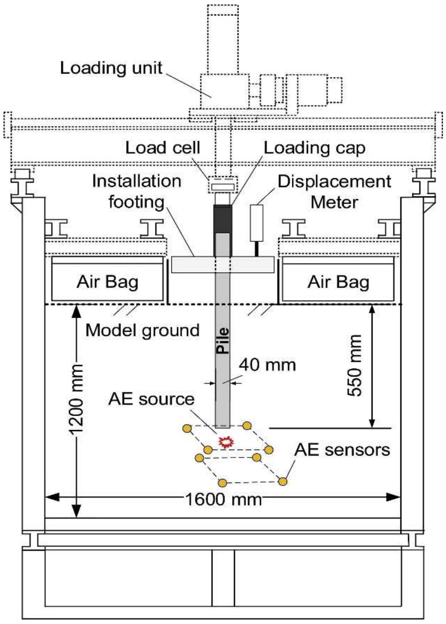

Fig. 11. Dimensions of the soil media, pile installation, and loading mechanism [23].

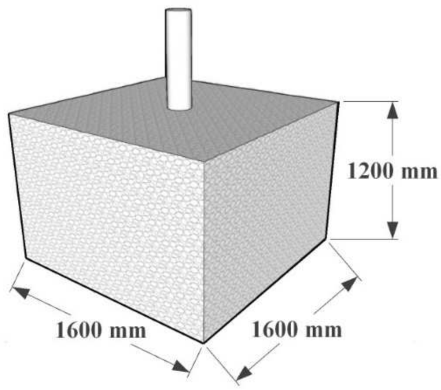

Fig. 12. Three-dimensional view of the model containing soil and penetrating pile.

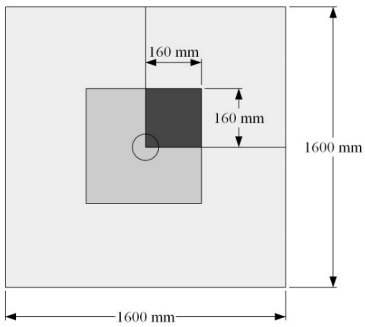

Fig. 13. Illustration of the symmetry of the model and the simulated segment.

Due to the geometric symmetry of the model in the length and width axes (Fig. 13), to minimize the computational volume, one-fourth of the soil and pile geometry is simulated. Moreover, by moving away from the center of the penetrating pile towards the walls of the soil-filled box reduces the intensity of stress changes caused by the pile penetration into the sandy soil. For this reason, the affected region of soil can be limited to a curtain domain. As a result, it is possible to neglect extra soil part during acoustic wave's propagation. Furthermore, since pile penetration occurs by overcoming the interparticle bonds of the sandy grains or by breaking the soil particles themselves, the origin of the acoustic signals with the nature of particle sliding and soil particle breakage will be under the pile tip.

Furthermore, the positions of the acoustic sensors used in this study are 70 mm away from the pile center in the longitudinal and transverse directions, and 90 mm in the vertical direction. The soil beyond the sensors has no impact on the received signals and only serves as a medium for wave propagation. As such, the simulation only considers the central core of the soil-filled box, neglecting the modeling of the entire three-dimensional geometry of the penetrating pile and the soil, as depicted in Fig. 13. (A cube with dimensions of 160 mm by 160 mm and a height of 800 mm). Ultimately, due to the extremely large computational domain and an extraordinarily high number of elements involved in simulating the entire domain, simulation in the actual dimensions was not feasible. Therefore, in the numerical simulation process of the laboratory model, geometric scaling techniques were utilized.

Table 4. Specifications of silica sand.

Internal friction angle (β)	Shear strain ratio (k)	Angle of dilation (Ψ)
46	1	7

Table 5. Aluminum pile material properties.

Material type	Young's modulus (MPa)	Poisson's ratio	Density (kg/m³)
Aluminum	70	0.35	2700

4.1.1. Soil parameters for acoustic wave propagation analysis

The elastic modulus of silicate sand according to [47] ranges from 40 to 80 MPa. The soil's Poisson's ratio is assumed to be 0.3. The Drucker-Prager model is used for soil plasticity behavior. According to the research by [48], the internal friction angle is 37 degrees. In this study, a linear Drucker-Prager model with hardening is employed. The Drucker-Prager friction angle (β) is obtained from the Eq. (11):

$$\tan\beta = \sqrt{3}\sin\phi \Big/ \sqrt{1+\frac{1}{3}\sin\varphi^2} \qquad \beta = 46.1 \tag{11}$$

The flow stress ratio (k) is assumed to be 1, and the dilation angle (Ψ) according to the research by [48] is 7 degrees. The parameters of the linear Drucker-Prager model are in accordance with Table 4.

Figure 14, based on the study by [49], has been used to introduce the hardness properties. The properties of the penetrating aluminum pile are also considered according to Table 5.

To simulate the stages of pile penetration into soil, three different steps have been employed. In the first step, a static general was used to apply the total weight of the assembly. The duration of this analysis step was 1 second. In the second step, a dynamic implicit analysis was conducted for 1 second to apply the loading on the pile. After applying the loading in the second step, a subsequent dynamic implicit with a duration of 50 microseconds was used in the third step.

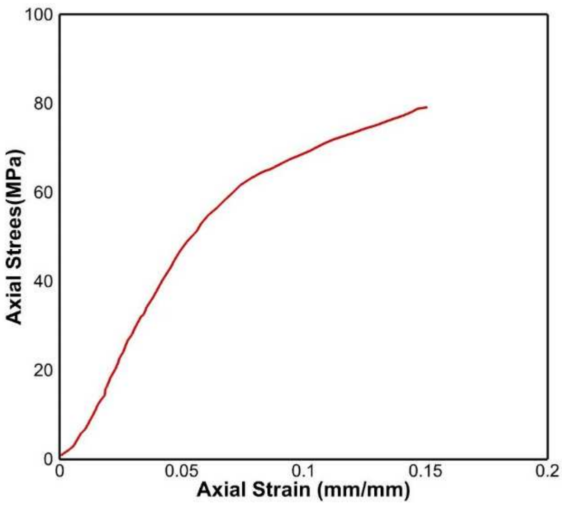

Fig. 14. Stress-strain curve of silica sand [49].

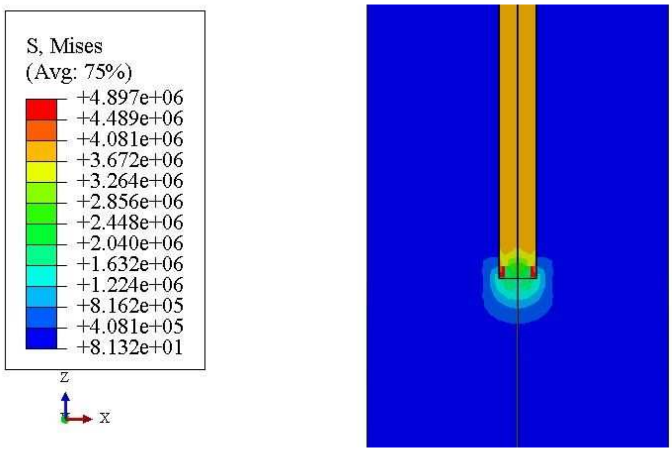

Fig. 15. Stress distribution within the soil and the penetrating pile.

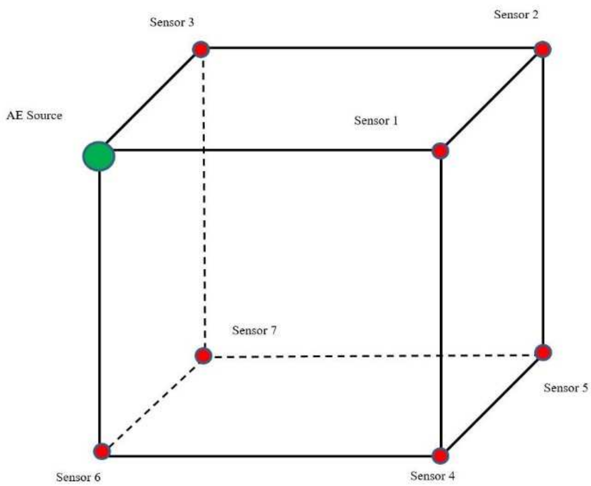

Fig. 16. Positions of the sensors and the acoustic source.

Table 6. Coordinates of acoustic sensors and source.

Sensor number	X-Coordinate	Y-Coordinate	Z-Coordinate
Sensor 1	0	0	0
Sensor 2	0	0.008	0
Sensor 3	-0.008	0.008	0
Sensor 4	0	0	-0.008
Sensor 5	0	-0.008	0.008
Sensor 6	-0.008	0	-0.008
Sensor 7	-0.008	-0.008	-0.008

Table 7. Coordinates of the acoustic source and computational source.

	X-Coordinate	Y-Coordinate	Z-Coordinate
Origin source [23]	-0.008	0	0
Localized source	-0.0082	-0.0001	0.0004

One crucial aspect to consider in the acoustic wave propagation analysis is the time steps and the sampling frequency for acquiring acoustic signals. Based on existing evidence, the sampling frequency should be at least twice the frequency of the acoustic signal propagation. According to available studies, the maximum frequency of the acoustic signal propagated in silica sand has been recorded as 200 kHz [22]. On the other hand, a time step of one microsecond has been considered for the third step of the analysis. In order to generate the gravitational volume force, in the first step of the analysis, a gravitational acceleration of 9.81 m/s² is applied vertically downward to the entire model. In the second step of the analysis, during the loading of the pile, to simulate the phenomenon of soil particle breakage and the movement of the pile within the soil mass, the penetration of the pile is simulated by applying a displacement control step. The penetration of the pile is simulated to a depth of 2 mm within one second in the vertical direction towards the pile tip.

In the third step, no external force is applied, and acoustic signals, generated due to the sliding and breakage of soil particles, are recorded and captured as elastic waves over a duration of 50 microseconds. According to existing research, the optimal position for receiving acoustic signals is at a distance half or equal to the diameter of the pile located beneath the pile tip [23]. Figure 15 illustrates the stress distribution after pile penetration. Acoustic waves are characterized as velocity change waves propagating perpendicular to the propagation plane in the materials [50]. The position of the acoustic source and the arrangement of the acoustic receivers are shown in Fig. 16. Furthermore, Table 6 specifies the coordinates of the acoustic sensors. In this model, 7 acoustic sensors are utilized to capture signals generated due to soil particle breakage, as schematically represented in Fig. 16. The received signals are also observed in Fig. 17.

To calculate the locations, initially, the first sensor is considered as the reference sensor, and the time differences of arrival of received signals are obtained using the cross-correlation method. Then, by assuming the speed of sound waves in the soil, the localization procedure is performed using the SI algorithm. Based on the above-mentioned localization algorithm, the location of the source of acoustic wave is provided in Table 7.

Since the obtained results imply, the maximum computational error in estimating the position of the acoustic wave source is 2.5%, indicating an acceptable accuracy in estimating the source location. For this reason, the localization algorithm employed in this contribution and the acoustic signal simulation technique are accurate and also could be extended to other numerical models.

4.2. Analyzing the factors affecting acoustic signals

In this section, the factors which influence the nature and form of acoustic waves resulting from the penetration of the pile into the soil are examined. During the penetration of the piles driven into the soil, obstacles in the path of pile movement, as well as various properties of the pile, can affect the type of waves emitted from the point of particle breakage. This section focuses on investigating the effects of soil elastic modulus, pile material, and the presence of obstacles in the path of pile penetration on the received signals. Analyzing such factors can be considered as a method of identifying inertial behavior during pile penetration into the soil. By analyzing the received signals from the pile penetration into the soil, a skilled operator can assess the conditions around the driven pile based on the analysis of the shape and magnitude of the received waves, leading to appropriate actions and decisions. After receiving the acoustic signals, which are in the form of velocity, they are transformed into the frequency domain using Fast Fourier Transformation (FFT). FFT is a tool that is used to decompose a signal into frequency components [51]. Therefore, the magnitude of the received acoustic signals is calculated and compared to study the influences of different conditions on pile penetration into the soil. Based on the existing experimental results, the elastic modulus of silica sand is considered to be between 40 to 80 MPa. To investigate the effect of soil elastic properties on the nature of acoustic waves, three samples of silica sand with elastic modulus of 40, 60, and 80 MPa are used. Additionally, to examine the influence of the pile material on the acoustic signals, three different pile samples made of aluminum, steel, and concrete materials are studied.

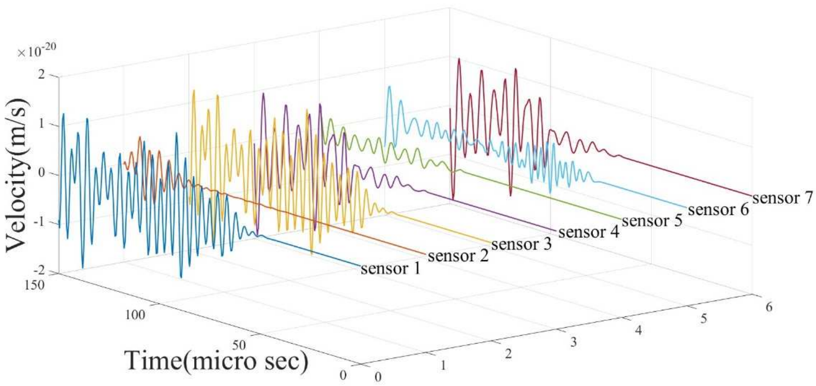

Fig. 17. Signals received from acoustic sensors.

It is worth mentioning that one of the very specific aspects in pile penetration in soil is timely identification of the presence of a hard obstacle or a void space (cavity) in front of the pile tip. Therefore, to investigate the presence of an obstacle in the path of pile penetration and its impact on the received acoustic signals, a concrete block under the pile tip and in the path of its penetration, as shown in Fig. 18, is considered. On the other hand, the presence of an empty space between the location of acoustic wave generation and the acoustic sensor, as depicted in Fig. 18, is also evaluated. For this purpose, the acoustic sensor is positioned at a distance of 40 mm in the longitudinal direction, 40 mm in the transverse direction, and 50 mm in the vertical direction from under the pile tip:

$$\text{Relative sensor coordinate} = \begin{bmatrix} +4\ cm \\ +4\ cm \\ -5\ cm \end{bmatrix} \tag{12}$$

First, the received propagating signals are analyzed, then the frequency domain analysis is performed, followed by signal decomposition and analysis.

In Fig. 19, the frequencies of the received signals resulting from the penetration of aluminum, concrete, and steel piles into soils with elastic moduli of 40, 60, and 80 MPa are observed.

4.2.1. The impact of soil elastic properties on acoustic waves

In Fig. 20, we investigate the effect of soil elastic properties on acoustic waves. The frequency of the signal resulting from the penetration of the pile into soils with 40, 60, and 80 MPa has been examined. In this study, the material of the pile is kept constant, and the variable is the type of soil.

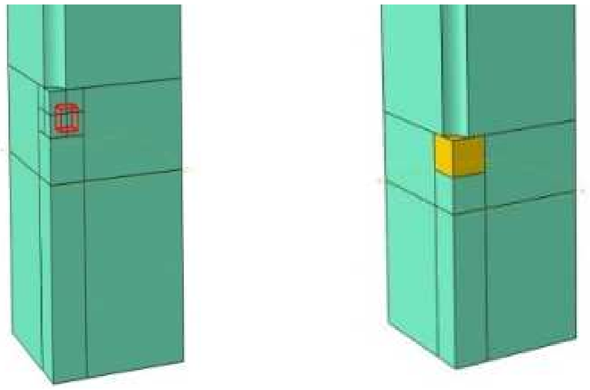

Fig. 18. The illustration of the obstacles between the sensor and the tip of the pile.

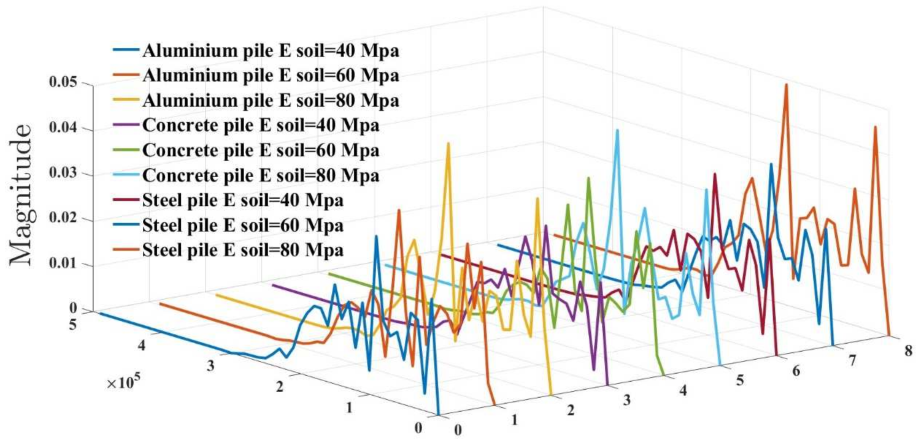

Fig. 19. Frequencies of received signals.

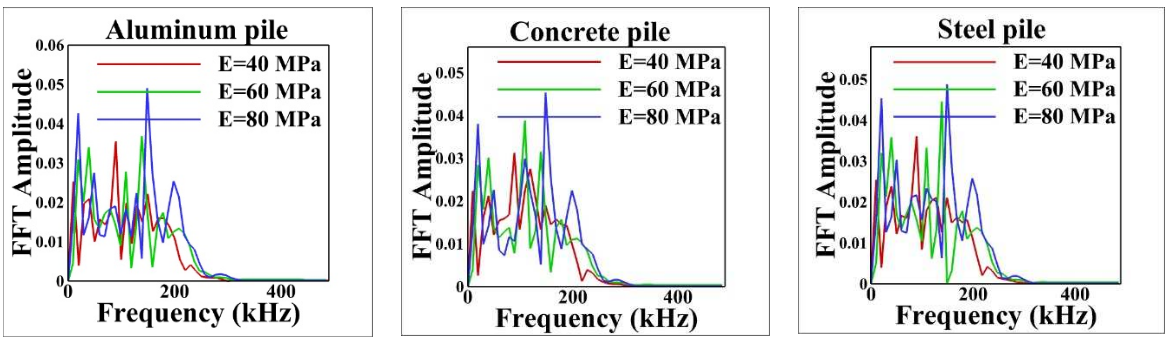

Fig. 20. The effect of soil elastic properties on acoustic waves.

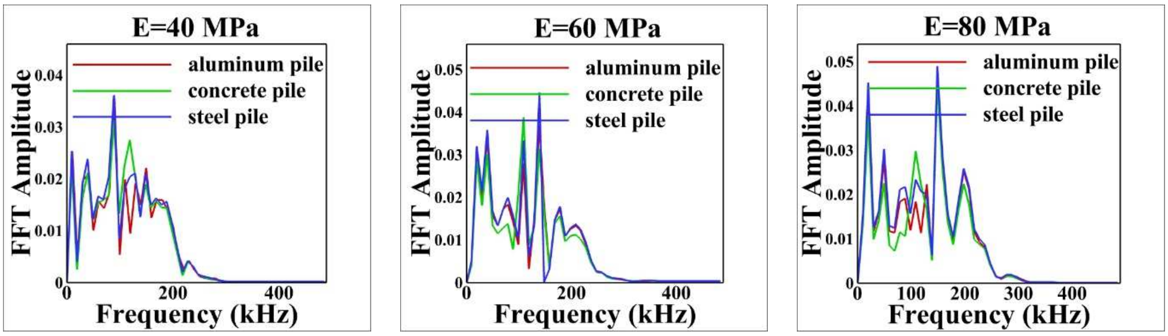

Fig. 21. The effect of the material of the penetrating pile on acoustic waves.

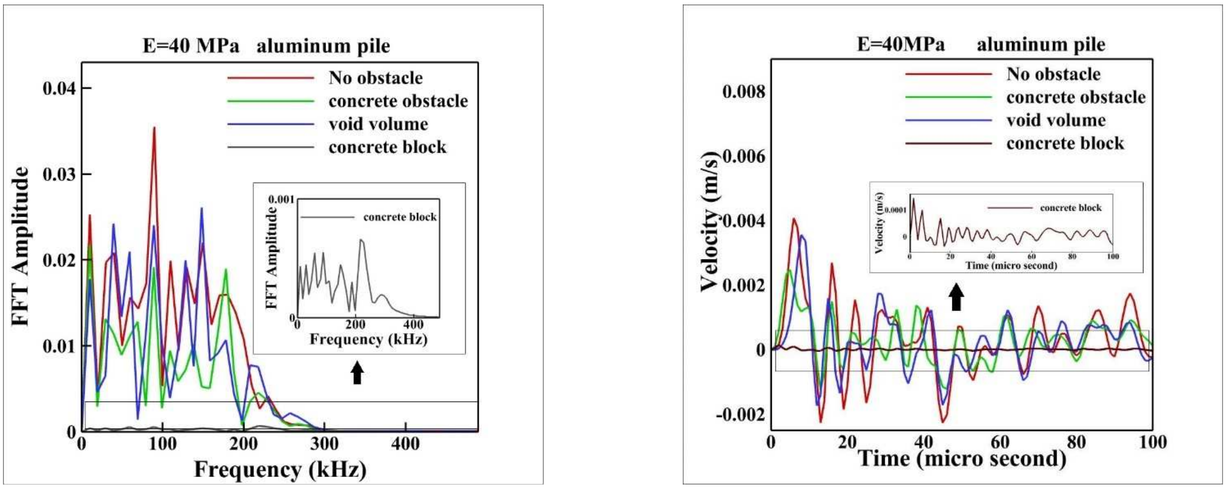

Fig. 22. Penetration of the pile with the presence of a concrete block under the pile and obstacle or void volume between pile tip and sensor in sand with an elastic modulus of 40 MPa.

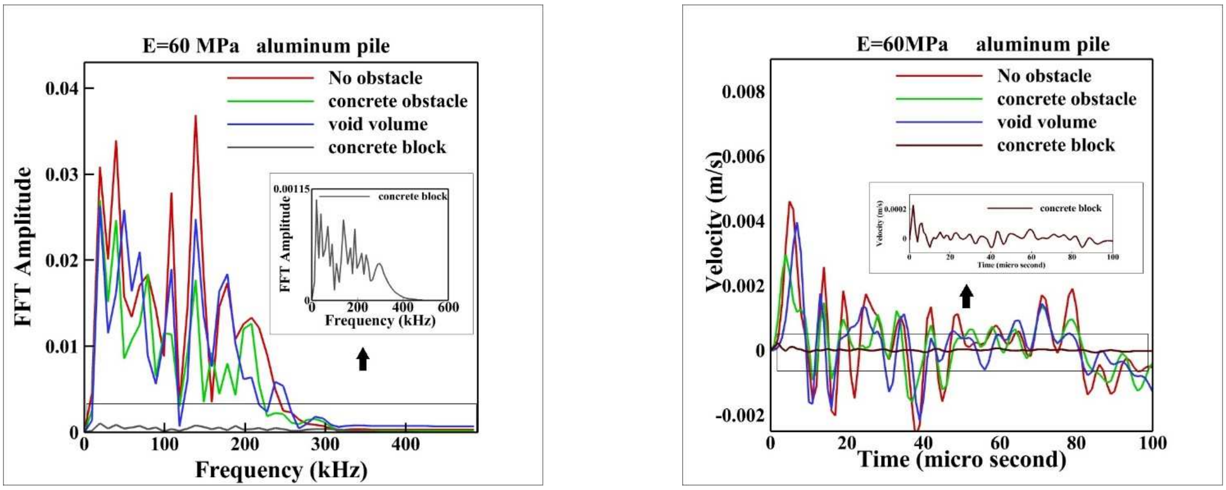

Fig. 23. Penetration of the pile with the presence of a concrete block under the pile and obstacle or void volume between pile tip and sensor in sand with an elastic modulus of 60 MPa.

The results obtained indicate that with an increase in the soil's elastic modulus, the magnitude of the acoustic wave frequencies also increases.

4.2.2. Investigating the effect of the material of the penetrating pile on acoustic waves

In Fig. 21, the effect of the material of the penetrating pile on acoustic waves is investigated. The frequency of the signal resulting from the penetration of aluminum, steel, and concrete piles into the soil has been examined. In this study, the soil type was constant, and the pile's material was variable.

The obtained results indicate that the penetrating pile's material does not have any significant effect on the frequency of the received acoustic signals.

4.2.3. Investigating the presence of an obstacle or void volume between the sensor and source of acoustic and a concrete block under the pile tip on acoustic waves

In this section, in addition to analyzing the received signal in the frequency domain, they have also been analyzed in the speed-time domain. The reason for this is that by comparing the frequencies of received signal in the normal state and the presence of an obstacle and a concrete block, the obtained results are ambiguous and no favorable conclusion can be made.

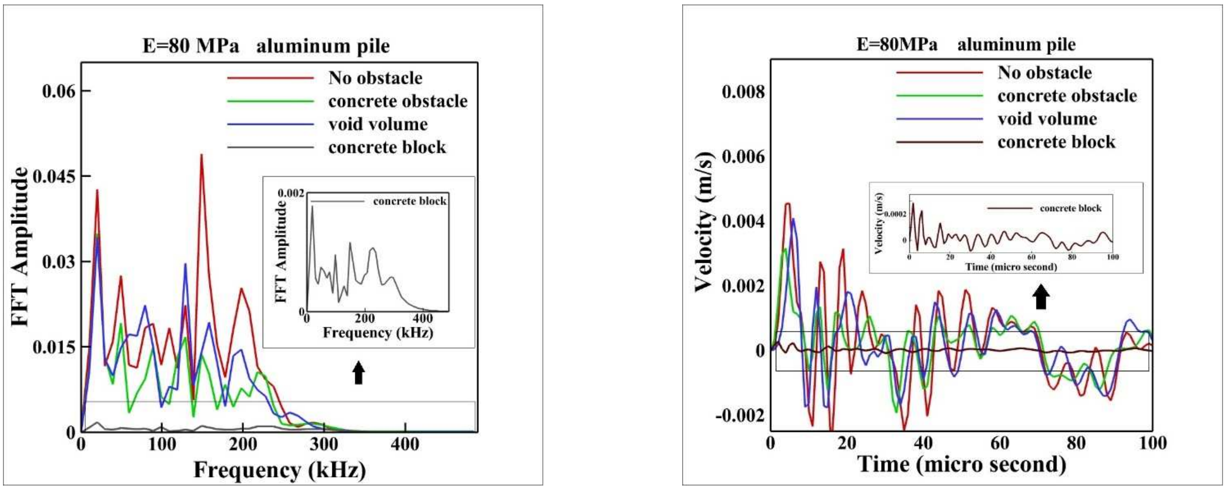

Fig. 24. Penetration of the pile with the presence of a concrete block under the pile and obstacle or void volume between pile tip and sensor in sand with an elastic modulus of 80 MPa.

Observations show that either the obstacle or concrete block subjected in the path of penetration of the pile, the dominant frequency of the received signal tends to zero. In this case, an abnormal situation was noticed which could not be analyzed through signal analysis in the frequency domain ,and the signal was investigated in the speed-time domain.

The speed of the received signal in the presence of void volume is not much different from the normal signal in terms of shape and maximum speed. The presence of an obstacle between the sensor and the acoustic source caused the maximum speed received to decrease (about half of the normal value). The presence of a concrete block under the pile tip causes a significant decrease in the maximum speed of the received signal and very different from normal state.

5. Conclusions

The applicability of passive monitoring on penetrating structural piles using acoustic emission technique was determined. This study provided deeper understanding on different situations against pile driving. The proposed method that based on numerical simulation may eliminate the high cost associated with acquiring the necessary hardware for receiving and analyzing the received signals. Another significant factor is the presence of noise in the received signal from the operational method, which can lead to the misinterpretation of the results. If these challenges are addressed, the proposed method can provide valuable insights into understanding the behavior of soil during pile penetration and the interaction between soil and pile for researchers in this field. The following are other conclusions drawn from this study:

1. The elastic modulus of the soil affects the received signal frequency; as the elastic modulus increases or, in other words, as the soil becomes harder, the received wave frequency also increases.
2. The type of penetrating pile does not have an effect on the received signal frequency; changing the pile type did not result in any variation in the received signal frequency.
3. A noticeable change in the received signal frequency, where the frequency tends towards zero or significantly deviates from the expected or predicted frequency, can be indicative of the presence of an obstacle in the path of the penetrating pile or the existence of an obstacle between the acoustic sensor and the tip of the pile.
4. Based on the obtained results and the comparisons with laboratory experimental methods for locating the place of soil particle breakage, we conclude that using the cross-correlation method for finding the Time Difference of Arrival (TDoA) of two signals, along with the SI (Spherical Interpolation) algorithm for acoustic source localization, is an appropriate and less error-prone method.

Furthermore, the findings of this research provide valuable information regarding the validity of Non-destructive method to obstacle detection. Also, the results may possibly be used by operators to monitor the situations against a penetrating member into a deeper layer with no subsurface exploration borehole.

Author Contributions

M. Rostami carried out the analysis, and participated in study design and manuscript preparation; A. Khademalrasoul suggested the original research methodology and results interpretation; A. Valipour developed the mathematical modeling and examined the theory validation. The manuscript was written through the contribution of all authors. All authors discussed the results, reviewed, and approved the final version of the manuscript.

Acknowledgments

We are deeply grateful to all reviewers for their valuable comments on the earlier version of this article. Additionally, we extend our appreciation to the editorial team at the Journal of Applied and Computational Mechanics, Shahid Chamran University of Ahvaz.

Conflict of Interest

The authors declared no potential conflicts of interest concerning the research, authorship, and publication of this article.

Funding

We sincerely acknowledge the Shahid Chamran University of Ahvaz for funding this study under grant number SCU.C1403.31071.

Data Availability Statements

The datasets generated and/or analyzed during the current study are available from the corresponding author on reasonable request.

Nomenclature

T	The signal duration	λ	Wavelength [m]
τ	Time delay	f	Frequency
R_{xy}	Correlation coefficient between two signals	υ	Acoustic wave velocity [m/s]
ρ	Density [kg/m^3]	E	Elastic modulus [Pa]

References

[1] Ghafghazi, M., Shuttle, D.A., DeJong, J.T., Particle breakage and the critical state of sand, *Soils and Foundations*, 54(3), 2014, 451-461.
[2] Xiao, Y., Meng, M., Daouadji, A., Chen, Q., Wu, Z., Jiang, X., Effects of particle size on crushing and deformation behaviors of rockfill materials, *Geoscience Frontiers*, 11(2), 2020, 375-388.
[3] Sadrekarimi, A., Effect of soil particle mineralogy on embankment dams, *Proceedings of the Institution of Civil Engineers - Geotechnical Engineering*, 165(3), 2012, 195-206.
[4] JARDINE, R.J., ZHU, B.T., FORAY, P., YANG, Z.X., Interpretation of stress measurements made around closed-ended displacement piles in sand, *Géotechnique*, 63(8), 2013, 613-627.
[5] Imre, B., Laue, J., Springman, S.M., Fractal fragmentation of rocks within sturzstroms: insight derived from physical experiments within the ETH geotechnical drum centrifuge, *Granular Matter*, 12(3), 2010, 267-285.
[6] Yasufuku, N., Hyde, A.F.L., Pile end-bearing capacity in crushable sands, *Géotechnique*, 45(4), 1995, 663-676.
[7] Simonini, P., Analysis of Behavior of Sand Surrounding Pile Tips, *Journal of Geotechnical Engineering*, 122(11), 1996, 897-905.
[8] Lobo-Guerrero, S., Vallejo, L., DEM analysis of crushing around driven piles in granular materials, *Géotechnique*, 55(8), 2005, 617-623.
[9] Zhang, C., Yang, Z.X., Nguyen, G.D., Jardine, R.J.,Einav, I., Theoretical breakage mechanics and experimental assessment of stresses surrounding piles penetrating into dense silica sand, *Géotechnique Letters*, 4(1), 2014, 11-16.
[10] Jin, Y.-F., Yin, Z.-Y., Wu, Z.-X., Daouadji, A., Numerical modeling of pile penetration in silica sands considering the effect of grain breakage, *Finite Elements in Analysis and Design*, 144, 2018, 15-29.
[11] Cuadra, J., Vanniamparambil, P.A., Hazeli, K., Bartoli, I., Kontsos, A., Damage quantification in polymer composites using a hybrid NDT approach, *Composites Science and Technology*, 83, 2013, 11-21.
[12] Kundu, T., Das, S., Jata, K.V., Point of impact prediction in isotropic and anisotropic plates from the acoustic emission data, *The Journal of the Acoustical Society of America*, 122(4), 2007, 2057-2066.
[13] Vanniamparambil, P.A., Bolhassani, M., Carmi, R., Khan, F., Bartoli, I., Moon, F.L., Hamid, A., Kontsos, A., A data fusion approach for progressive damage quantification in reinforced concrete masonry walls, *Smart Materials and Structures*, 23(1), 2014, 015007.
[14] Niccolini, G., Durin, G., Lacidogna, G., Manuello, A., Carpinteri, A., AE monitoring of the Syracuse Athena Temple: Scale invariance in the timing of ruptures, *Experimental Mechanics on Emerging Energy Systems and Materials, Volume 5: Proceedings of the 2010 Annual Conference on Experimental and Applied Mechanics*, Springer, 2011.
[15] Manuello, A., Marmo, F., Melchiorre, J., Investigating and monitoring central nave vaults of the Turin Cathedral with Acoustic Emissions and Thrust Network Analysis, *Developments in the Built Environment*, 18, 2024, 100434.
[16] Niu, Y., Hu, Y.-J., Wang, J.-G., Cracking characteristics and damage assessment of filled rocks using acoustic emission technology, *International Journal of Geomechanics*, 23(4), 2023, 04023013.
[17] Ma, G., Xie, Y., Long, G., Tang, Z., Tang, C., Wang, H., Wei, Y., Li, J., Experimental study on acoustic emission and surface morphology characteristics of concrete under different fracture modes, *Theoretical and Applied Fracture Mechanics*, 123, 2023, 103702.
[18] Verstrynge, E., Van Steen, C., Vandecruys, E., Wevers, M., Steel corrosion damage monitoring in reinforced concrete structures with the acoustic emission technique: A review, *Construction and Building Materials*, 349, 2022, 128732.
[19] Sause, M., Horn, S., Simulation of Lamb Wave Excitation for Different Elastic Properties and Acoustic Emission Source Geometries, *Journal of Acoustic Emission*, 28, 2010, 109-121.
[20] Xu, J., Wang, W., Han, Q., Liu, X., Damage pattern recognition and damage evolution analysis of unidirectional CFRP tendons under tensile loading using acoustic emission technology, *Composite Structures*, 238, 2020, 111948.
[21] Gunerkar, R., Jalan, A., Classification of ball bearing faults using vibro-acoustic sensor data fusion, *Experimental Techniques*, 43, 2019, 635-643.
[22] Mao, W., Towhata, I., Monitoring of single-particle fragmentation process under static loading using acoustic emission, *Applied Acoustics*, 94, 2015, 39-45.
[23] Mao, W., Aoyama, S., Towhata, I., A study on particle breakage behavior during pile penetration process using acoustic emission source location, *Geoscience Frontiers*, 11(2), 2020, 413-427.
[24] Capelli, A., Kapil, J.C., Reiweger, I., Or, D., Schweizer, J., Speed and attenuation of acoustic waves in snow: Laboratory experiments and modeling with Biot's theory, *Cold Regions Science and Technology*, 125, 2016, 1-11.
[25] Qi, G., Attenuation of acoustic emission body waves in acrylic bone cement and synthetic bone using wavelet time-scale analysis, *Journal of Biomedical Materials Research*, 52(1), 2000, 148-156.
[26] Hesser, D.F., Mostafavi, S., Kocur, G.K., Markert, B., Identification of acoustic emission sources for structural health monitoring applications based on convolutional neural networks and deep transfer learning, *Neurocomputing*, 453, 2021, 1-12.
[27] Melchiorre, J., D'Amato, L., Agostini, F., Rizzo, A.M., Acoustic emission onset time detection for structural monitoring with U-Net neural network architecture, *Developments in the Built Environment*, 18, 2024, 100449.
[28] Yang, G., Yan, Y., Wang, H., Shen, X., Improved robust TOA-based source localization with individual constraint of sensor location uncertainty, *Signal Processing*, 196, 2022, 108504.
[29] Carpinteri, A., Xu, J., Lacidogna, G., Manuello, A., Reliable onset time determination and source location of acoustic emissions in concrete structures, *Cement and Concrete Composites*, 34(4), 2012, 529-537.
[30] Sedlak, P., Hirose, Y., Enoki, M., Acoustic emission localization in thin multi-layer plates using first-arrival determination, *Mechanical Systems and Signal Processing*, 36(2), 2013, 636-649.
[31] Melchiorre, J., Manuello Bertetto, A., Rosso, M.M., Marano, G.C., Acoustic emission and artificial intelligence procedure for crack source localization, *Sensors*, 23(2), 2023, 693.
[32] Kocur, G.K., Kumar, B., Markert, B., TDOA-based localization of cracking sound events with minimal-error microphone subsets, *NDT & E International*, 147, 2024, 103211.
[33] Jiao, J., Zhang, J., Ren, Y., Li, G., Wu, B., He, C., Sparse representation of acoustic emission signals and its application in pipeline leak location, *Measurement*, 216, 2023, 112899.
[34] Chen, L., Liu, Y., Kong, F., He, N., Acoustic Source Localization Based on Generalized Cross-correlation Time-delay Estimation, *Procedia Engineering*, 15, 2011, 4912-4919.
[35] Rinehart, A.J., McKenna, S.A., Dewers, T.A., Using wavelet covariance models for simultaneous picking of overlapping P-and S-wave arrival times in noisy single-component data, *Seismological Research Letters*, 87(4), 2016, 893-900.
[36] Smith, J., Abel, J., Closed-form least-squares source location estimation from range-difference measurements, *IEEE Transactions on Acoustics, Speech, and Signal Processing*, 35(12), 1987, 1661-1669.

[37] Schau, H., Robinson, A., Passive source localization employing intersecting spherical surfaces from time-of-arrival differences, *IEEE Transactions on Acoustics, Speech, and Signal Processing*, 35(8), 1987, 1223-1225.
[38] Wu, C., Deng, H., Yan, S., Sun, X., Ji, Y., Xiao, J., Indoor Acoustic Localization by Using Chan Algorithm, *2021 4th International Conference on Information Communication and Signal Processing (ICICSP)*, Shanghai, China, 2021.
[39] Kovavisaruch, L., Ho, K.C., Modified Taylor-series method for source and receiver localization using TDOA measurements with erroneous receiver positions, *2005 IEEE International Symposium on Circuits and Systems (ISCAS)*, Kobe, Japan, 2005.
[40] Friedlander, B., A passive localization algorithm and its accuracy analysis, *IEEE Journal of Oceanic Engineering*, 12(1), 1987, 234-245.
[41] Yoon, D.-J., Weiss, W.J., Shah, S.P., Assessing damage in corroded reinforced concrete using acoustic emission, *Journal of Engineering Mechanics*, 126(3), 2000, 273-283.
[42] John, R., Shah, S.P., Mixed-mode fracture of concrete subjected to impact loading, *Journal of Structural Engineering*, 116(3), 1990, 585-602.
[43] Yazid, A., Abdelkader, N., Abdelmadjid, H., A state-of-the-art review of the X-FEM for computational fracture mechanics, *Applied Mathematical Modelling*, 33(12), 2009, 4269-4282.
[44] Feng, J., Qin, Y., Liskiewicz, T.W., Beake, B.D., Wang, S., Crack propagation of a thin hard coating under cyclic loading: Irreversible cohesive zone model, *Surface and Coatings Technology*, 426, 2021, 127776.
[45] Beliaev, M., Semenov, A., Semenov, S., Benin, A., Simulation of Pulling the Reinforcing Bar from Concrete Block with Account of Friction and Concrete Damage, *MATEC Web of Conferences*, Petersburg, Russia, 2016.
[46] Mao, W., Yang, Y., Lin, W., Aoyama, S., Towhata, I., High Frequency Acoustic Emissions Observed during Model Pile Penetration in Sand and Implications for Particle Breakage Behavior, *International Journal of Geomechanics*, 18(11), 2018, 04018143.
[47] Yanai, M., Ichikawa, N., Muto, N., Ishiyama, K., Uniaxial Compression Test with Varying Silica Sand Content, Particle size and Temperature, *GEOMATE Journal*, 19(74), 2020, 210-215.
[48] Yu, F.-W., Su, L.-J., Particle breakage and the mobilized drained shear strengths of sand, *Journal of Mountain Science*, 13(8), 2016, 1481-1488.
[49] Suescun-Florez, E., Kashuk, S., Iskander, M., Bless, S., Predicting the uniaxial compressive response of granular media over a wide range of strain rates using the strain energy density concept, *Journal of Dynamic Behavior of Materials*, 1(3), 2015, 330-346.
[50] Cuadra, J., Vanniamparambil, P., Servansky, D., Bartoli, I., Kontsos, A., Acoustic emission source modeling using a data-driven approach, *Journal of Sound and Vibration*, 341, 2015, 222-236.
[51] Zhao, Y., Lv, H., Li, J., Zhu, L., High performance and resource efficient FFT processor based on CORDIC algorithm, *EURASIP Journal on Advances in Signal Processing*, 2022(1), 2022, 23.

ORCID iD

Mohammad Rostami https://orcid.org/0009-0003-1759-8408
Abdolghafour Khademalrasoul https://orcid.org/0000-0001-7917-7535
Ali Valipour https://orcid.org/0000-0002-8326-9843

How to cite this article: Rostami M., Khademalrasoul A., Valipour A. Application of Acoustic Emission for Diagnostic Pile Penetration by Consideration of Soil Particle Breakage, *J. Appl. Comput. Mech.*, 12(1), 2026, 60–73. https://doi.org/10.22055/jacm.2025.47278.4687